Giant Enhancement in the Thermal Responsivity of Microelectromechanical Resonators by Internal Mode Coupling

Ya Zhang,[1,*] Ryoka Kondo,[2] Boqi Qiu,[2] Xin Liu,[4] and Kazuhiko Hirakawa[2,3,†]

[1] *Institute of Engineering, Tokyo University of Agriculture and Technology, Koganei-shi, Tokyo 184-8588, Japan*
[2] *Institute of Industrial Science, University of Tokyo, 4-6-1 Komaba, Meguro-ku, Tokyo 153-8505, Japan*
[3] *Institute for Nano Quantum Information Electronics, University of Tokyo, 4-6-1 Komaba, Meguro-ku, Tokyo 153-8505, Japan*
[4] *Beijing-Dublin International College and Institute of Theoretical Physics, Beijing University of Technology, 100 Pingleyuan, 100124 Beijing, People's Republic of China*

(Received 20 March 2020; revised 25 April 2020; accepted 1 June 2020; published 8 July 2020)

We report on a giant enhancement in the thermal responsivity of doubly clamped GaAs microelectromechanical-system- (MEMS) beam resonators by using the internal-mode-coupling effect. This is achieved by coupling the fundamental bending mode with the fundamental torsional mode of the MEMS-beam resonators through the cubic Duffing nonlinearity. In the mode-coupling regime, we find that when the input heat to the MEMS resonators is modulated at a particular frequency, the resonance-frequency shift caused by heating can be enhanced by almost 2 orders of magnitude. The observed effect is promising for realization of high-sensitivity thermal sensing by use of MEMS resonators, such as ultrasensitive terahertz detection at room temperature.

DOI: 10.1103/PhysRevApplied.14.014019

Microelectromechanical system (MEMS) resonators [1–3] are very attractive for sensing applications owing to their intrinsic high sensitives. The high mechanical quality factors of MEMS resonators enable the detection of small changes in the resonance frequency, which can be used for detecting changes in mass [4–6], charge [7,8], spin orientation [9–11], temperature [12,13], and infrared radiation [14]. A resonant MEMS sensor is often described by a spring-mass model. The sensing target, such as molecules, charges, and temperature, modulates either the spring constant or the mass of the system, and the signal is detected as a shift in the resonance frequency. The responsivity is simply determined by how much the sensing target modulates the spring constant or the mass. Such a simple operation principle makes it difficult to dramatically increase the responsivity of MEMS sensors.

The mode-coupling effect in MEMS resonators has attracted considerable interest since it changes the properties of MEMS resonators substantially. A vibrational mode is coupled with a higher mode through internal resonance when their frequencies fulfill the integer ratio of 1:N, where N is the nonlinear order of the MEMS resonator [15–19]. In the mode-coupling regime, the energy is transferred from the externally driven mode to other modes. The use of such an effect was proposed for realization of frequency stabilization [15] and synchronization [20], vibrational-energy harvesting [21], energy-dissipation control [22,23], and the detection of higher resonance modes [24]. The mode-coupling effect is also very attractive for sensing applications owing to its rich features with regard to the oscillation amplitude and frequency of MEMS resonators. Indeed, it was used to increase the responsivities in mass sensing applications [25,26], in which a steady-state feature of the internal mode resonance was used. However, dynamical effects of the internal mode resonance on MEMS sensors have been much less explored [27].

Here we report on a giant enhancement in the thermal responsivity of doubly clamped GaAs MEMS-beam resonators [28–30] by using the internal-mode-coupling effect. This is achieved by coupling the fundamental bending mode with the fundamental torsional mode of MEMS-beam resonators through the cubic Duffing nonlinearity. In the mode-coupling regime, we find that when the input heat to the MEMS resonators is modulated at a particular frequency, the resonance-frequency shift caused by heating can be enhanced by almost 2 orders of magnitude. The observed effect is promising for realization of high-sensitivity thermal sensing by use of MEMS resonators, such as ultrasensitive terahertz detection at room temperature, and also has potential for other sensing applications.

*zhangya@go.tuat.ac.jp
†hirakawa@iis.u-tokyo.ac.jp

 © 2020 American Physical Society

We fabricate doubly clamped GaAs MEMS-beam resonators by using a modulation-doped (Al, Ga)As/GaAs heterojunction grown by molecular-beam epitaxy [31]. After growing a 200-nm-thick GaAs buffer layer and a 3-μm-thick $Al_{0.7}Ga_{0.3}As$ sacrificial layer on a (100)-oriented semi-insulating GaAs substrate, we form the beam layer by depositing a 1-μm-thick GaAs layer. We subsequently grow a 20-nm-thick Si-doped GaAs layer, a 70-nm-thick $Al_{0.3}Ga_{0.7}As$ layer, and a 10-nm-thick GaAs capping layer. The suspended beam structure is formed by our selectively etching the sacrificial layer with dilute hydrofluoric acid. On both ends of the beam, we fabricate an Ohmic contact and a surface Schottky gate to form piezoelectric capacitors to drive the beam [28,30,31]. An ac voltage is applied to one of the piezoelectric capacitors to drive the beam and the induced resonant beam motion is monitored by a laser Doppler vibrometer. The resonance signal is fed to a phase-locked loop (PLL) to provide feedback control to maintain self-oscillation and read the resonance amplitude and frequency by use of the built-in lock-in detection function of the PLL. On the MEMS beam, we deposit a 10-nm-thick NiCr layer, whose sheet resistance is approximately 1000 Ω/□, as a heater to thermally modulate the resonance frequencies and also calibrate the responsivity of the MEMS resonator. All the measurements are performed in a vacuum (approximately 10^{-4} Torr) at room temperature.

To induce internal mode coupling via the cubic Duffing nonlinearity in doubly clamped MEMS-beam resonators, we need two resonance modes whose resonance frequencies fulfill the relationship $f_1/f_2 = 1{:}3$. Here we use the fundamental bending mode (f_b) and the fundamental torsional mode (f_t) to create the internal mode coupling. The ratio (f_b/f_t) can be controlled, because f_b is determined mainly by the length of the MEMS beam, whereas f_t is determined mainly by the width. We design doubly

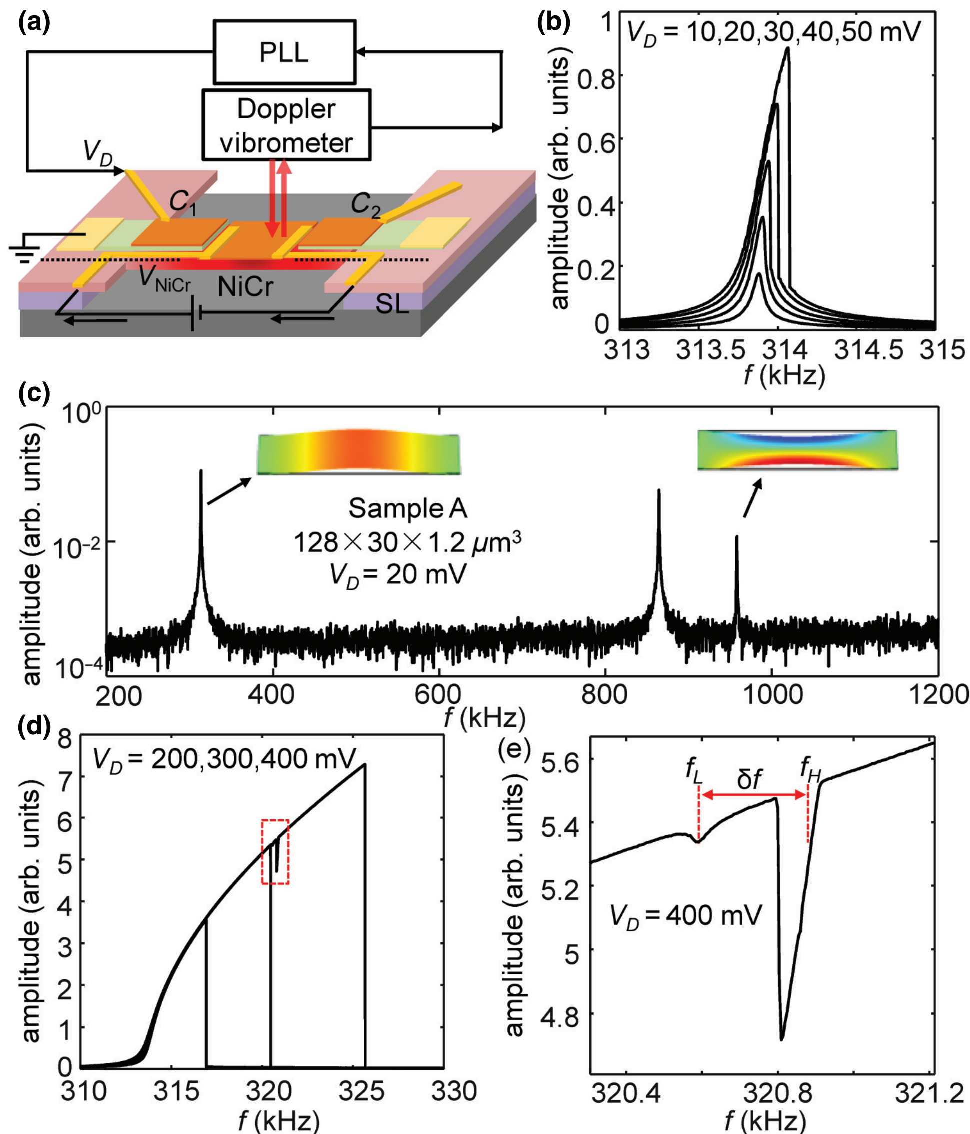

FIG. 1. (a) The measurement setup. An ac voltage is applied to one of the piezoelectric capacitors to drive the beam and the induced resonant beam motion is monitored by a laser Doppler vibrometer. The motion signal is fed to a PLL circuit to provide feedback control to maintain self-oscillation. The PLL is also used as a lock-in amplifier to measure the resonance spectrum. (b) Measured resonance spectra of the first bending mode at various driving voltages ($V_D = 10$–50 mV) applied to the piezoelectric capacitor. (c) Measured spectrum for the first three modes (i.e., the first bending mode, the second bending mode, and the first torsional mode). The inset shows the mode shapes of the first bending mode and the first torsional mode calculated by the finite-element method. (d) Measured resonance spectra when $V_D = 200, 300, 400$ mV. (e) Enlargement of the spectrum in the mode-coupling region marked by a dotted rectangle in (d). Two clear drops in the amplitude appear in the spectrum at approximately 320.6 kHz and approximately 320.9 kHz, which are denoted as f_L and f_H, respectively. δf is the difference between f_L and f_H. SL, sacrificial layer.

clamped MEMS-beam resonators with a length of 128 μm, a width of 30 μm, and a thickness of 1.2 μm in such a way that f_b is slightly smaller than one third of f_t. We apply an ac driving voltage ($V_{D)}$ of 20 mV to a MEMS-beam resonator (sample A) and sweep the driving frequency. The resonance spectrum is measured by use of a PLL with lock-in detection as a built-in function, as schematically shown in Fig. 1(a). The PLL is also used to provide feedback control to maintain self-oscillation, as we reported elsewhere [30]. Figure 1(c) plots the measured spectrum for the first three modes (i.e., the first bending mode, the second bending mode, and the first torsional mode). Note that $f_b \approx 313.8$ kHz and $f_t = 958.0$ kHz. The inset in Fig. 1(c) shows the mode shapes of the first bending mode and the first torsional mode calculated by the finite-element method. Figure 1(b) shows the measured resonance spectra of the first bending mode at various driving voltages ($V_D = 10$–50 mV) applied to the piezoelectric capacitor [31]. The quality factor of the resonance is about 5000. When the first bending mode is driven into the nonlinear Duffing oscillation regime ($V_D > 20$ mV), f_b increases with increasing driving amplitude, which is due to the hardening effect of the GaAs MEMS beam. By using this effect, we tune f_b to make it approach $f_t/3 \approx 320$ kHz.

Figure 1(d) shows the measured resonance spectrum when V_D = 200, 300, 400 mV. When f_b is increased to about 320 kHz, a small reduction in the resonance amplitude is observed in the spectrum, indicating that the vibrational energy of the fundamental mode decreases in this condition. Figure 1(e) shows an enlargement of the spectrum in the mode-coupling region marked by the dotted red rectangle in Fig. 1(d). Two clear drops in the amplitude appear at approximately 320.6 kHz and approximately 320.9 kHz, suggesting that internal mode coupling is formed between the driven fundamental mode and a higher mode. Since the internal mode coupling in MEMS-beam resonators usually arises from cubic term nonlinearity, we identify the higher mode in this mode coupling to be the first torsional mode ($f_t = 958.0$ kHz). When the two modes couple with each other, they are renormalized into two new eigenmodes, f_L and f_H (f_L is the lower-frequency coupled mode and f_H is the higher-frequency coupled mode). These two new coupled modes appear as two dips in the resonance spectrum of the f_b mode at around 320 kHz ($f_L \approx 320.6$ kHz and $f_H \approx 320.9$ kHz) as shown in Fig. 1(e), since the vibrational energy is transferred to the f_t mode at these frequencies. The frequency difference between f_L and f_H (δf) is approximately 300 Hz for sample A. Internal-mode-coupling behavior is also observed in another sample (sample B) and the frequency difference δf is approximately 500 Hz (see the Appendix).

To study the effect of internal mode coupling on the thermal responsivity of the MEMS resonator, we apply a dc voltage to the NiCr heater to generate heat on the MEMS beam and measure f_b as a function of the heating power, P. Figure 2 shows f_b for sample A as a function of P at various values of V_D (283–424 mV). The red and black curves show the data when P is swept from 0 to 0.25 mW (forward) and from 0.25 to 0 mW (backward), respectively. In general, f_b is smoothly reduced when P is increased due to thermal expansion of the MEMS beam, which has been used for standard thermal sensing [28,30]. When P is swept backward, f_b shows a plateau at $f_1 = 320.6$ kHz, which corresponds to the first amplitude drop in Fig. 1(e). When P is swept forward, on the other hand, a kink is observed at the frequency of the second amplitude drop ($f_2 \approx 320.9$ kHz) in Fig. 1(e), as indicated by a dashed red arrow. This behavior is explained by the interplay between the mechanical nonlinearity and the internal-mode-coupling effect, which was proposed to achieve frequency stabilization in MEMS resonators [15]. The frequency plateau makes the thermal responsivity vanishingly small.

Next, we apply a small amount of modulated heat ($P \approx 25$ nW) to the MEMS beam of sample A when the sample is operated in the mode-coupling condition. Because of the frequency stabilization in the mode-coupling region, the frequency shift of the MEMS bolometer is vanishingly small when the heat modulation frequency, f_m, is low (less than 100 Hz). However, when the heat is modulated at a particular frequency (approximately 300 Hz) under the internal-mode-coupling condition, we observe a huge peak in the frequency shift, as shown by the red and blue curves in Fig. 3(a). For comparison, the black curve in Fig. 3(a) shows the frequency shift with the same heating power when the MEMS resonator is operated outside the mode-coupling region. When $f_m \approx 300$ Hz, the heat-induced frequency shifts in

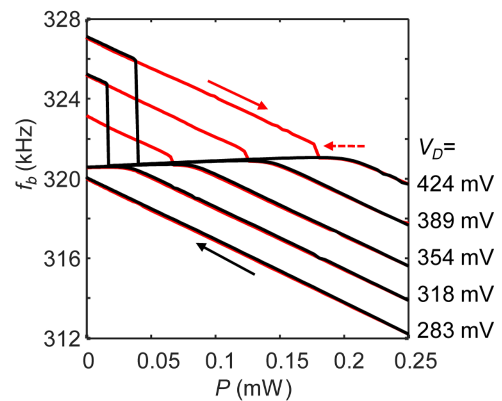

FIG. 2. Resonance frequency f_b for sample A measured as a function of the input heating power P at various values of V_D (283–424 mV). The red and black curves show the data when P is swept from 0 to 0.25 mW (forward) and from 0.25 to 0 mW (backward), respectively. The red and black arrows indicate the sweep directions in the measurements. The dashed red arrow indicates the position of the kink in f_b.

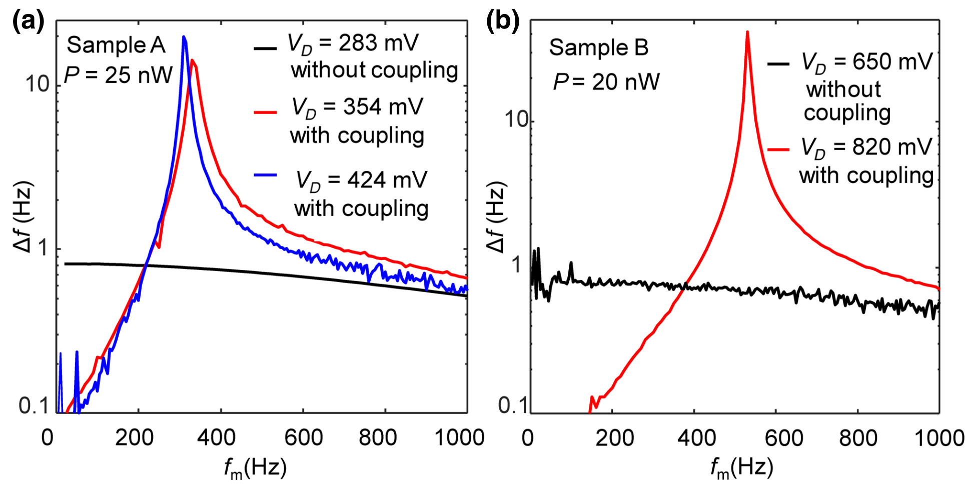

FIG. 3. (a) Thermally induced frequency shift, Δf, for sample A as a function of the modulation frequency of the applied heat (approximately 25 nW) measured at various driving voltages, V_D. The black, blue, and red curves plot the results when $V_D = 283$, 354, and 424 mV, respectively. In the mode-coupling region ($V_D = 354$ and 424 mV), the frequency shift is vanishingly small when the heat modulation frequency is low (less than 100 Hz), but shows a large peak when the heat is modulated at a particular frequency (approximately 300 Hz). The black curve ($V_D = 283$ mV) shows the frequency shift measured outside the mode-coupling region. (b) Thermally induced Δf for sample B as a function of the modulation frequency of the applied heat (approximately 20 nW) measured at various values of V_D. The black and red curves plot the results when $V_D = 650$ mV (outside the mode-coupling region) and 820 mV (inside the mode-coupling region), respectively. Δf reaches its maximum when the heat is modulated at approximately 530 Hz.

the mode-coupling region are 14 Hz ($V_D = 354$ mV) and 20 Hz ($V_D = 424$ mV), which are, respectively, 17.5 and 25.0 times higher than that (approximately 0.8 Hz) outside the mode-coupling region ($V_D = 283$ mV). The different frequency shifts at various driving voltages suggest that the enhancement factor can be modulated by controlling the mode-coupling condition.

Figure 3(b) shows the shift in the resonance frequency for sample B measured inside and outside the mode-coupling region when $P = 20$ nW is applied to the MEMS beam. When the MEMS resonator is operated outside the mode-coupling region ($V_D = 650$ mV), the frequency shift is about 0.7 Hz and almost does not depend on f_m. However, when the MEMS resonator is operated in the mode-coupling region ($V_D = 820$ mV), the frequency shift shows a large peak of more than 40 Hz when $f_m \approx 530$ Hz, which is more than 60 times higher than that in the uncoupled condition.

We find that f_m that induces a large thermal responsivity agrees well with the frequency difference, δf, between the two dips in the resonance spectra (f_L and f_H). This suggests that the greatly enhanced thermal responsivity originates from coherent energy transfer between the two coupled modes. To understand the mechanism, we measure how f_b develops for the modulated heat input. Figure 4(b) plots the shift in f_b as a function of time when a small amount of heat of approximately 20 nW (ac amplitude) at a modulation frequency of approximately 530 Hz is applied to the MEMS resonator. Figure 4(a) shows the waveform of the heat pulses fed to the MEMS beam. As seen, the frequency shift of f_b is both positive and negative and gradually becomes very large. The time constant is on the order of approximately 100 ms. This is very different from the thermal response of MEMS resonators without mode coupling, where the resonance frequency decreases only due to thermal expansion when heat is applied to the MEMS beam, as we reported before [30].

In the mode-coupled condition, the MEMS resonator is driven at f_L, which corresponds to the first dip in Fig. 1(e). The pumped f_L mode coherently transfers its vibrational energy to the f_H mode through the parametric driving effect [32–35]. The parametrically excited f_H mode forms a beating signal together with the f_L mode, which periodically modulates the amplitude of the bending motions in the f_L and f_H modes, as schematically shown in Fig. 4(c). We have bending motions at f_L and f_H, and their constructive and destructive interferences modulate the amplitude of the bending motion at the frequency $\delta f = f_H - f_L$. Then, f_b is periodically modulated through the amplitude-frequency coupling that arises from the Duffing nonlinearity. Since the amplitude change of the bending motion caused by the interference is proportional to the amplitude of the f_H mode, the periodic frequency shift becomes a sensor for measuring the amplitude of the f_H mode [36]. Therefore, the enhanced frequency shift in Fig. 4(a) shows that the amplitude of the f_H mode is increased by the parametric drive, until it becomes saturated due to the damping process.

Finally, we discuss how the present mode-coupling effect improves the detector performance. Figure 5(a)

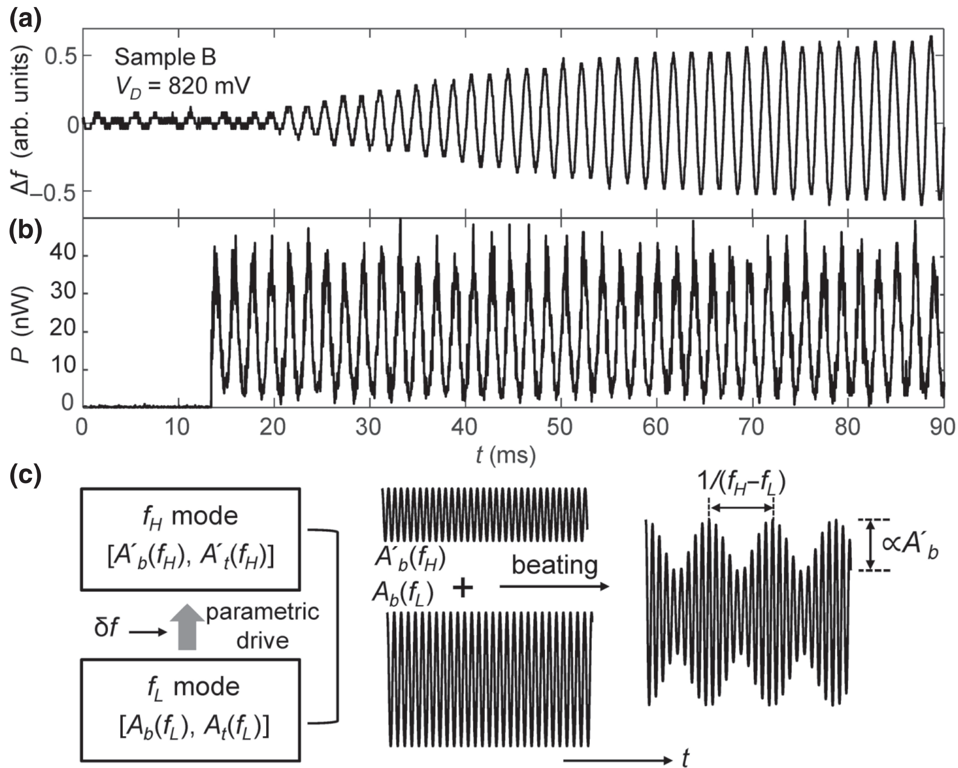

FIG. 4. (a) Waveform of the input heat pulses fed to the MEMS beam. The applied heat power is approximately 20 nW (ac amplitude) and is modulated at approximately 530 Hz. (b) Time trace of Δf measured when a small amount of heat is applied to sample B. The MEMS resonator is operated in the mode-coupling regime ($V_D = 820$ mV). (c) The beating effect between the f_L and f_H modes. In the mode-coupling condition, the bending mode and the torsional mode are renormalized into new coupled modes at frequencies f_L and f_H. The f_L and f_H modes consist of the bending component (A_b, A_b') and the torsional component (A_t, A_t'). When the MEMS resonator is driven at f_L by our causing bending motion using the piezoelectric capacitor and, in addition, heat is applied periodically to the beam at frequency $\delta f = f_H - f_L$, the f_L mode coherently transfers its vibrational energy to the f_H mode through the parametric driving effect. The parametrically excited f_H mode generates a beating signal with the f_L mode, which periodically modulates the amplitude of the bending component.

shows the frequency shift measured in the mode-coupling region (450 Hz $< f_m <$ 600 Hz) for sample B when P is varied from 2 to 20 nW. Figure 5(b) plots the shift in the resonance frequency, Δf, determined from the curves plotted in Fig. 5(a) as a function of P. When $P \leq 10$ nW, Δf increases almost linearly with increasing P. However, when $P > 10$ nW, Δf gradually deviates from the linear increase. We estimated the thermal responsivity, $R \equiv \Delta f / P f_b \approx 10\,000$ W^{-1}, by using a linear fitting to Δf for $P \leq 10$ nW, as indicated by the dotted line in Fig. 5(b). The obtained R in the mode-coupling condition is almost 2 orders of magnitude larger than that in the uncoupled region.

In Fig. 5(c), we plot the spectral density of frequency noise, n_f, in (red) and outside (black) the mode-coupling region. As seen, at $f_m = 530$ Hz, where a large enhancement in the thermal responsivity is observed, n_f also becomes larger ($n_f \approx 50$ mHz/$\sqrt{\text{Hz}}$) when the MEMS resonator is operated under the mode-coupling condition ($V_D = 820$ mV). Such enhancement in n_f is not observed when the mode coupling is absent. Therefore, the noise equivalent power (NEP $\equiv n_f / R f_b$) is not increased as much as R.

In thermal sensors, there is a fundamental limit for NEP, namely, the thermal fluctuation limit, which is determined by the random transfer of thermal phonons between the MEMS beam and the thermal reservoir (the substrate in our device) and can be calculated as [37]

$$\text{NEP}_{\text{TF}} \approx (4 k_B T^2 G_T)^{0.5} \approx 20\ \text{pW}/\sqrt{\text{Hz}} \quad \text{at } T = 300\ \text{K}, \tag{1}$$

where k_B is the Boltzmann constant and T the temperature. In Fig. 5(d), we plot NEP as a function of f_m in (red) and outside (black) the mode-coupling region. When the resonator is operated in the mode-coupling region ($V_D = 820$ mV), NEP becomes as small as 23 pW/$\sqrt{\text{Hz}}$ at $f_m = 530$ Hz. This NEP is close to the value of the thermal fluctuation limit, NEP_{TF}, which is indicated by a dotted red line in Fig. 5(d). When

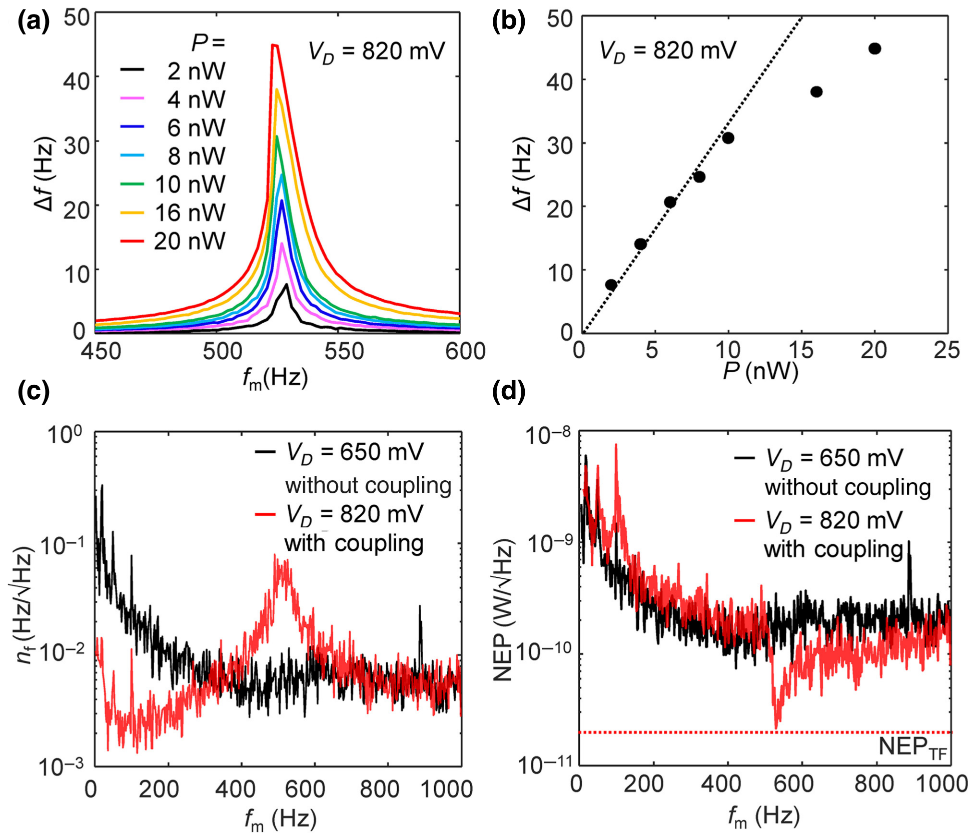

FIG. 5. (a) Thermally induced frequency shift in sample B measured in the mode-coupling region when the heating power $P = 2$, 4, 6, 8, 10, 16, and 20 nW and the heat modulation frequency, f_m, is swept from 450 to 600 Hz. (b) Peak frequency shift Δf in the mode-coupling region as a function of P. The dotted line indicates a linear fit to Δf for $P \leq 10$ nW to estimate the thermal responsivity. (c) Spectral density of frequency noise, n_f, measured when $V_D = 650$ mV (outside the mode-coupling region; black) and when $V_D = 820$ mV (in the mode-coupling region; red). (d) NEP as a function of f_m when $V_D = 650$ mV (outside the mode-coupling region; black) and when $V_D = 820$ mV (in the mode coupling region; red). The dotted red line indicates the thermal fluctuation limit for NEP.

compared with NEP ≈ 150 pW/$\sqrt{\text{Hz}}$ without mode coupling ($V_D = 650$ mV), the increase in NEP is about 6–7 times. Although the mode-coupling effect can increase R by almost 2 orders of magnitude, the increase in NEP is partly compensated by the increase in n_f. However, if extrinsic noise such as noise from amplifiers is dominant, the increase in NEP will be governed by R.

In summary, we demonstrate a giant enhancement in the thermal responsivity of doubly clamped GaAs MEMS resonators using the internal-mode-coupling effect. The coupling between the fundamental bending mode and the fundamental torsional mode is formed by using the cubic Duffing nonlinearity in the system. When static heat is applied to the MEMS beam, the frequency shift from the thermal effect is strongly suppressed, giving a vanishingly small thermal responsivity. However, when we apply modulated heat to the MEMS beam at a particular modulation frequency of several hundreds of hertz, the thermally induced frequency shift is enhanced by almost 2 orders of magnitude, giving a giant enhancement in the thermal responsivity of the MEMS resonator. The enhancement is due to the energy transfer between two renormalized coupled modes by parametric driving. The observed effect is promising for realization of high-sensitivity thermal sensing applications using MEMS resonators, such as ultrasensitive terahertz detection at room temperature, and it also has potential for other sensing applications.

ACKNOWLEDGMENTS

We are grateful to Y. Arakawa and H. Yamaguchi for fruitful discussions. This work was partly supported by JST Collaborative Research Based on Industrial Demand, a MEXT Grant-in-Aid for Scientific Research on Innovative Areas “Science of Hybrid Quantum Systems” (Grant No. 15H05868), and KAKENHI from JSPS (Grants No. 15K13966 and No. 19K15023). Grants from the Precise Measurement Technology Promotion Foundation and the Murata Science Foundation are also acknowledged.

APPENDIX A: THE INTERNAL-MODE-COUPLING BEHAVIOR OBSERVED IN SAMPLE B

Similarly to what we observed in sample A, internal-mode-coupling behavior is also observed in another sample (sample B), which has a resonance frequency slightly different from that in sample A due to fluctuations in the fabrication process. For sample B, the first bending mode and the first torsional mode have resonance frequencies of 307.6 kHz (f_b) and 944.4 kHz (f_t), respectively. By strongly driving the fundamental mode into the nonlinear regime, we observe two drops in the resonance amplitude as marked by the dotted red rectangle in Fig. 6(a), in a similar manner as observed for sample A. Figure 6(b) shows an enlargement of the marked

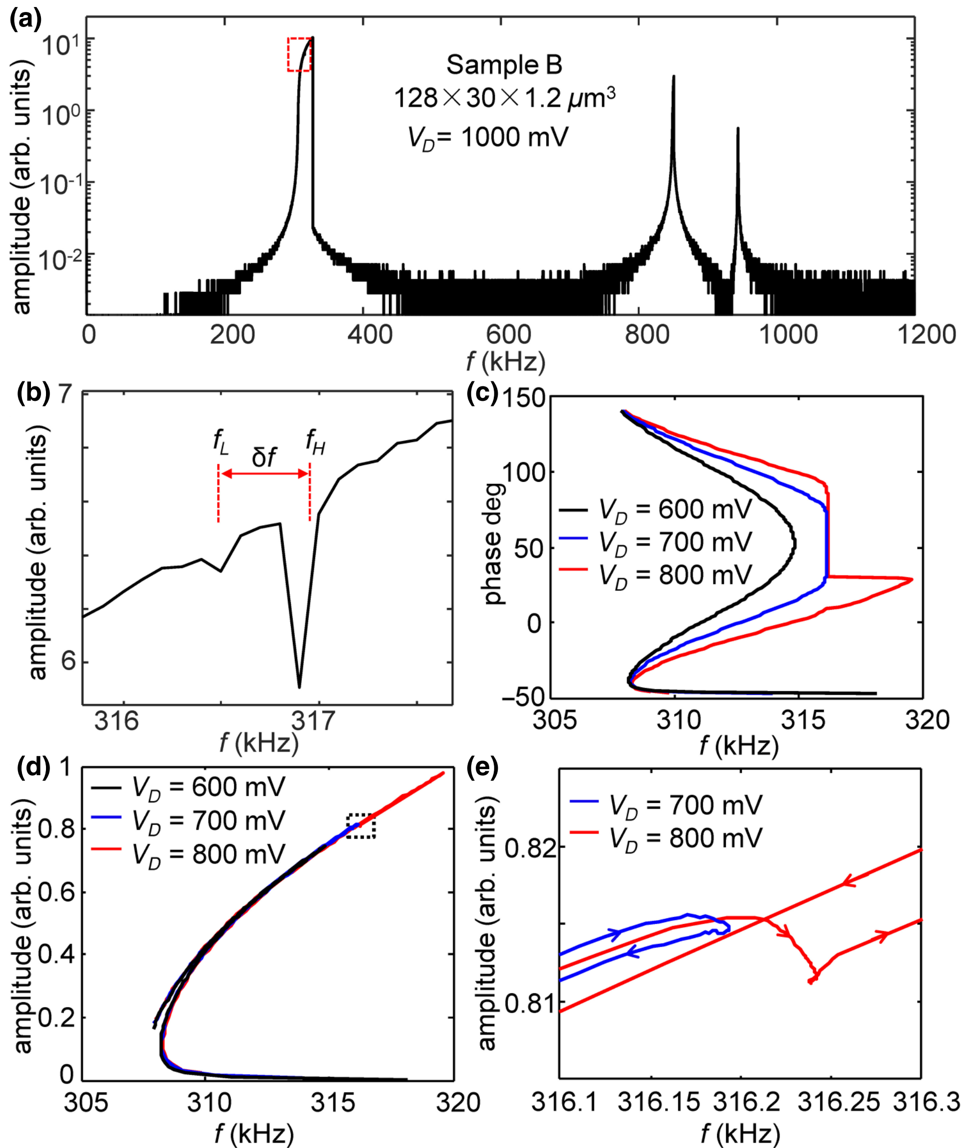

FIG. 6. Fig. 6(a) Measured resonance spectrum of sample B for the first three modes (i.e., the first bending mode, the second bending mode, and the first torsional mode). (b) Enlargement of the region marked by a dotted rectangle in the spectrum shown in (a). Two clear drops in amplitude appear in the spectrum at approximately 316.5 kHz and approximately 317 kHz, which are denoted as f_L and f_H, respectively. δf is the difference between f_L and f_H. (c) Phase spectra measured at various driving voltages ($V_D = 600$, 700, and 800 mV). The phase sweep is performed with a PLL. (d) Resonance spectra measured at various driving voltages ($V_D = 600$, 700, and 800 mV). (e) Enlargement of the mode-coupling region marked by a dotted box in (d). Drops in the resonance amplitude are observed.

region in Fig. 6(a). As seen, two drops appear at approximately 316.5 kHz and approximately 317 kHz, giving the frequency difference $\delta f \approx 500$ Hz. We perform closed-loop measurements by using the PLL, where we fix V_D and sweep the phase of V_D with respect to the vibrational phase measured by a Doppler vibrometer. Figure 6(a) plots the resonance frequency as a function of the phase of V_D when V_D is set to be 600, 700, and 800 mV. As f_b approaches 316 kHz, f_b is stabilized and is not affected by the phase shift. The same frequency-stabilization effect was reported and well explained in Ref. [15]. Figure 6(d) shows the resonance-amplitude spectra. Figure 6(e) is an enlargement of Fig. 6(d) for the mode-coupling region. As can be seen, drops in the resonance amplitude are observed, suggesting that the vibrational energy of the lower-resonance mode is reduced by the mode-coupling effect.

[1] K. Ekinci and M. Roukes, Nanoelectromechanical systems, Rev. Sci. Instrum. **76,** 061101 (2005).

[2] A. Boisen, S. Dohn, S. S. Keller, S. Schmid, and M. Tenje, Cantilever-like micromechanical sensors, Rep. Prog. Phys. **74,** 036101 (2011).

[3] A. N. Cleland, *Foundations of Nanomechanics: From Solid-State Theory to Device Applications* (Springer Science & Business Media, 2013).

[4] K. L. Ekinci, X. M. H. Huang, and M. L. Roukes, Ultrasensitive nanoelectromechanical mass detection, Appl. Phys. Lett. **84,** 4469 (2004).

[5] Y. T. Yang, C. Callegari, X. L. Feng, K. L. Ekinci, and M. L. Roukes, Zeptogram-scale nanomechanical mass sensing, Nano Lett. **6,** 583 (2006).

[6] K. Jensen, K. Kim, and A. Zettl, An atomic-resolution nanomechanical mass sensor, Nat. Nanotech. **3,** 533 (2008).

[7] A. N. Cleland and M. L. Roukes, A nanometre-scale mechanical electrometer, Nature **392**, 160 (1998).
[8] R. Knobel, C. S. Yung, and A. N. Cleland, Single-electron transistor as a radio-frequency mixer, Appl. Phys. Lett. **81**, 532 (2002).
[9] D. Rugar, R. Budakian, H. Mamin, and B. Chui, Single spin detection by magnetic resonance force microscopy, Nature **430**, 329 (2004).
[10] S. C. Masmanidis, H. X. Tang, E. B. Myers, M. Li, K. De Greve, G. Vermeulen, W. Van Roy, and M. L. Roukes, Nanomechanical Measurement of Magnetostriction and Magnetic Anisotropy in (Ga, Mn) As, Phys. Rev. Lett. **95**, 187206 (2005).
[11] K. Onomitsu, I. Mahboob, H. Okamoto, Y. Krockenberger, and H. Yamaguchi, Ferromagnetic-induced component in piezoresistance of GaMnAs, Phys. Rev. B **87**, 060410(R) (2013).
[12] A. K. Pandey, O. Gottlieb, O. Shtempluck, and E. Buks, Performance of an AuPd micromechanical resonator as a temperature sensor, Appl. Phys. Lett. **96**, 203105 (2010).
[13] T. Larsen, S. Schmid, L. Grönberg, A. Niskanen, J. Hassel, S. Dohn, and A. Boisen, Ultrasensitive string-based temperature sensors, Appl. Phys. Lett. **98**, 121901 (2011).
[14] X. C. Zhang, E. B. Myers, J. E. Sader, and M. L. Roukes, Nanomechanical torsional resonators for frequency-shift infrared thermal sensing, Nano Lett. **13**, 1528 (2013).
[15] D. Antonio, D. H. Zanette, and D. López, Frequency stabilization in nonlinear micromechanical oscillators, Nat. Commun. **3**, 806 (2012).
[16] C. Samanta, P. Yasasvi Gangavarapu, and A. Naik, Nonlinear mode coupling and internal resonances in MoS2 nanoelectromechanical system, Appl. Phys. Lett. **107**, 173110 (2015).
[17] D. A. Czaplewski, S. Strachan, O. Shoshani, S. W. Shaw, and D. López, Bifurcation diagram and dynamic response of a MEMS resonator with a 1: 3 internal resonance, Appl. Phys. Lett. **114**, 254104 (2019).
[18] A. Afaneh and R. Ibrahim, Nonlinear response of an initially buckled beam with 1: 1 internal resonance to sinusoidal excitation, Nonlinear Dynamics **4**, 547 (1993).
[19] S. Houri, D. Hatanaka, M. Asano, and H. Yamaguchi, Demonstration of Multiple Internal Resonances in a Microelectromechanical Self-Sustained Oscillator, Phys. Rev. Appl. **13**, 014049 (2020).
[20] D. Pu, X. Wei, L. Xu, Z. Jiang, and R. Huan, Synchronization of electrically coupled micromechanical oscillators with a frequency ratio of 3: 1, Appl. Phys. Lett. **112**, 013503 (2018).
[21] C. Lan, W. Qin, and W. Deng, Energy harvesting by dynamic unstability and internal resonance for piezoelectric beam, Appl. Phys. Lett. **107**, 093902 (2015).
[22] C. Chen, D. H. Zanette, D. A. Czaplewski, S. Shaw, and D. López, Direct observation of coherent energy transfer in nonlinear micromechanical oscillators, Nat. Commun. **8**, 1 (2017).
[23] J. Güttinger, A. Noury, P. Weber, A. M. Eriksson, C. Lagoin, J. Moser, C. Eichler, A. Wallraff, A. Isacsson, and A. Bachtold, Energy-dependent path of dissipation in nanomechanical resonators, Nat. Nanotech. **12**, 631 (2017).
[24] A. B. Arı, MÇ Karakan, C. Yanık, İİ Kaya, and M. S. Hanay, Intermodal Coupling as a Probe for Detecting Nanomechanical Modes, Phys. Rev. Appl. **9**, 034024 (2018).
[25] T. Zhang, X. Wei, Z. Jiang, and T. Cui, Sensitivity enhancement of a resonant mass sensor based on internal resonance, Appl. Phys. Lett. **113**, 223505 (2018).
[26] C. R. Kirkendall, D. J. Howard, and J. W. Kwon, Internal resonance in quartz crystal resonator and mass detection in nonlinear regime, Appl. Phys. Lett. **103**, 223502 (2013).
[27] C. Zhao, X. Zhou, M. Pandit, G. Sobreviela, S. Du, X. Zou, and A. Seshia, Toward High-Resolution Inertial Sensors Employing Parametric Modulation in Coupled Micromechanical Resonators, Phys. Rev. Appl. **12**, 044005 (2019).
[28] Y. Zhang, Y. Watanabe, S. Hosono, N. Nagai, and K. Hirakawa, Room temperature, very sensitive thermometer using a doubly clamped microelectromechanical beam resonator for bolometer applications, Appl. Phys. Lett. **108**, 163503 (2016).
[29] Y. Zhang, S. Hosono, N. Nagai, and K. Hirakawa, Effect of buckling on the thermal response of microelectromechanical beam resonators, Appl. Phys. Lett. **111**, 023504 (2017).
[30] Y. Zhang, S. Hosono, N. Nagai, S.-H. Song, and K. Hirakawa, Fast and sensitive bolometric terahertz detection at room temperature through thermomechanical transduction, J. Appl. Phys. **125**, 151602 (2019).
[31] I. Mahboob and H. Yamaguchi, Bit storage and bit flip operations in an electromechanical oscillator, Nat. Nanotech. **3**, 275 (2008).
[32] M. Zalalutdinov, A. Olkhovets, A. Zehnder, B. Ilic, D. Czaplewski, H. G. Craighead, and J. M. Parpia, Optically pumped parametric amplification for micromechanical oscillators, Appl. Phys. Lett. **78**, 3142 (2001).
[33] H. Yamaguchi, GaAs-based micro/nanomechanical resonators, Semicond. Sci. Technol. **32**, 103003 (2017).
[34] I. Mahboob, K. Nishiguchi, H. Okamoto, and H. Yamaguchi, Phonon-cavity electromechanics, Nat. Phys. **8**, 387 (2012).
[35] H. Yamaguchi and I. Mahboob, Parametric mode mixing in asymmetric doubly clamped beam resonators, New J. Phys. **15**, 015023 (2013).
[36] H. J. R. Westra, M. Poot, H. S. J. Van Der Zant, and W. J. Venstra, Nonlinear Modal Interactions in Clamped-Clamped Mechanical Resonators, Phys. Rev. Lett. **105**, 117205 (2010).
[37] F. J. Low, Low-temperature germanium bolometer, J. Opt. Soc. Am. **51**, 1300 (1961).